Modeling and Estimation of the Humans' Effect on the CO_2 Dynamics Inside a Conference Room

Kevin Weekly, Nikolaos Bekiaris-Liberis, Ming Jin, and Alexandre M. Bayen

***Abstract*— We develop a data driven, *partial differential equation-ordinary differential equation* model that describes the response of the *carbon dioxide* (CO_2) dynamics inside a conference room, due to the presence of humans, or of a user-controlled exogenous source of CO_2. We conduct three controlled experiments to develop and tune a model whose output matches the measured output concentration of CO_2 inside the room, when known inputs are applied to the model. In the first experiment, a controlled amount of CO_2 gas is released inside the room from a regulated supply, and in the second and third experiments, a known number of humans produce a certain amount of CO_2 inside the room. For the estimation of the exogenous inputs, we design an observer, based on our model, using measurements of CO_2 concentrations at two locations inside the room. We perform several simulation studies for the illustration of our results.**

***Index Terms*— Data-driven model, distributed delay, distributed parameter systems, human occupancy estimation, identifier design, indoor carbon dioxide (CO_2) dynamics, observer design, partial differential equation-ordinary differential equation (PDE-ODE) cascades.**

I. Introduction

A. Motivation

REDUCING energy demand is an important component of smart building research. Building energy use is responsible for an increasing proportion of the total energy demand. In the United States, the proportion of building electricity consumption has raised to 40% in 2005, from 33% in 1980 [18] and in Singapore, buildings accounted for 31% of the total electricity consumption for the year 2007 [37]. Thus, the problem of reducing building energy demand through advanced technologies and finer-tuned services has been the focus of ongoing research. The knowledge of occupancy levels in discrete zones within a building offers the potential of significant energy savings when coupled with zonal control of building services [1], [14], [19], which is a motivation for the work presented in this paper.

A relatively unexplored approach for estimating the number of humans occupying discrete zones of office spaces, such as, for example, a conference room within a larger office space, is to model and estimate the effect of the carbon dioxide (CO_2) that is produced from humans on the total CO_2 concentration in the specific discrete zone (i.e., the conference room). The reason is that humans are the primary producers of CO_2 inside a building [40] and that CO_2 sensors are widely deployed in smart buildings (since CO_2 is an important quantity to observe to manage occupant comfort [40] and since this quantity can be measured using cheap sensors).

The development of model-based estimation algorithms allow the robust (for example, to model uncertainties), automatic, and real-time estimation of certain unmeasured quantities. In the present case, developing an estimation algorithm for the CO_2 concentration that is produced by people in an office space is important because not only it is a first step toward real-time estimation of human occupancy in buildings, but also the developed algorithms could be utilized complementarily to applications such as, for example, contaminant source identification, in which such an information is needed in real time [48].

Modeling CO_2 dynamics is challenging, due to the complexity of air dynamics. Most recently, two categories of models are used: zonal models and *computational fluid dynamics* (CFD) models. CFD models provide the most rich and detailed view of air motion in a space, however, they are beset by arduous work in modeling the physical space (e.g., providing locations of all walls, furniture, and occupants) and identifying all parameters that are needed for the model. CFD models also suffer from lengthy computation times needed to solve the necessary partial differential equations (PDEs) at a high resolution, especially near boundaries [31], [39]. Zonal models relate the movement of air between discrete and well-mixed spaces, such as rooms and parts of rooms. In general, zonal models rely on ordinary differential equation (ODE) mass balance laws between these spaces, which, in comparison with the CFD models, can be solved very quickly [31]. However, this comes at the expense of not modeling the distributed nature of airborne contaminant transfer within a single space, and complex local phenomena such as jets of air coming from a vent [32].

Yet, for designing and implementing estimation algorithms for the CO_2 concentration, it is desirable to develop a simple, and at the same time, accurate PDE-based model that retains the distributed character of the system. Based on this model, one can then design an observer for estimating the unknown CO_2 input that is produced from humans. The observer design is desirable to be developed using the minimum

Manuscript received September 24, 2014; accepted November 21, 2014. Date of publication January 8, 2015; date of current version August 7, 2015. Manuscript received in final form December 12, 2012. This work was supported by the National Research Foundation of Singapore through a grant to the Berkeley Education Alliance for Research in Singapore for the Singapore-Berkeley Building Efficiency and Sustainability in the Tropics Program. Recommended by Associate Editor A. Alessandri.

The authors are with the Department of Electrical Engineering and Computer Sciences, University of California at Berkeley, Berkeley, CA 94720 USA (e-mail: kweekly@eecs.berkeley.edu; bekiaris-liberis@berkeley.edu; jinming@berkeley.edu; bayen@berkeley.edu).

Color versions of one or more of the figures in this paper are available online at http://ieeexplore.ieee.org.

Digital Object Identifier 10.1109/TCST.2014.2384002

number of sensors, to reduce the cost and increase the reliability.

B. Literature

Our modeling and estimation efforts for the CO_2 produced by humans in a room lie in the general study of airborne contaminant modeling and estimation in indoor spaces. There is a wide variety of models from mass-conservation-based ODE models [36] to highly detailed CFD models for indoor airflow [15], [28]. The choice of model is often dependent on the end application and what information is available. For instance, low-order ODE models may not operate at fine enough spatial resolution to be useful, whereas a detailed CFD model may be too complex for designing the estimation or identification algorithms. Techniques for the estimation of the concentration of contaminants emitted from a source in indoor environments exist in [4], [13], [21], [30], [38], [41], [47], and [50]. In particular, [27] and [49] are dealing with the estimation of CO_2 emitted by humans for the purposes of occupancy detection. Our method is unique in that we derive a simple, data-driven PDE-ODE coupled system, and recast the problem of identification of the unknown CO_2 input produced by humans as a problem of state estimation of the PDE-ODE system.

Boundary observers for some classes of PDEs are constructed in [16], [17], [24], [25], and [43] via backstepping. In [34], this methodology is applied for the estimation of the state-of-charge of batteries. Observer designs for time-delay systems with unknown inputs are presented in [2], [6], and [22].

C. Results

We conduct three experiments. In the first, a regulated amount of CO_2 gas is released in the conference room for specific time periods, while CO_2 concentrations are measured at various locations in the room. We use these measurements to develop a model that reproduces the measured CO_2 concentration, given the known CO_2 release. In the second experiment, we monitor the evolution of the CO_2 concentrations at three different locations in the room, as two researchers enter and exit the room at recorded times. The purpose is to verify the model that we develop in the first experiment under a CO_2 input that is generated by humans. In the third experiment, we again monitor the evolution of the CO_2 concentration in the conference room due to the changes in human occupancy, but for a larger number of occupants, to validate our model for situations with more than two occupants.

We model the dynamics of the CO_2 concentration in the room using a convection PDE with a source term, which models the effect of the CO_2 that is generated by humans. The source term is the output of a linear, time invariant, scalar, and stable ODE system whose input represents the unknown humans' emission rate of CO_2 inside the room. We assume further that the unmeasured CO_2 emission rate from the humans has the form of a piecewise constant signal. This formulation is based on our experimental observation that the response of the CO_2 concentration in the room due to changes of the human's CO_2 input has some similarities with the step response of a low-pass filter.

Fig. 1. Office space under study.

We design an observer for the overall PDE-ODE system using boundary measurements (at the air supply and the air return). The observer estimates the unknown input from the humans, as well as the overall PDE state of our model. Our observer design is based on the results from [7] for linear systems with distributed sensor delays.

D. Structure of This Paper

The structure of this paper proceeds as follows. In Section II, we describe the three ground truth experiments undertaken to drive and validate our model and estimation algorithms. In Section III, we derive a coupled PDE-ODE model for the dynamics of the CO_2 concentration in the room. In Section IV, we design an observer for the estimation of the total CO_2 that is generated by humans.

Notation: The spatial $L_2(0, 1)$ norm is denoted by $\|\cdot\|$. The initial condition of a function $u(x, t)$, where $(x, t) \in [0, 1] \times [0, +\infty)$ is denoted by $u_0(x) = u(x, 0)$, for all $x \in [0, 1]$.

II. Experimental Setup

Our experimental work takes place in a 44 m^3 conference room, shown in Fig. 1. The room is completely interior within the building and has no outside walls. On the ceiling there is one air supply vent with a diffuser and protective grate, and there is also an air return vent with a protective grate.

We measure CO_2 concentration using the K-30 sensor module [26] (Fig. 2), which comes with specifications of ± 30 ppm $\pm 3\%$ accuracy and repeatability of ± 20 ppm $\pm 1\%$. Since we expect the nominal CO_2 concentrations of the room to be no more than 1800 ppm, this gives a repeatability error bound of ± 38 ppm.

The American Society of Heating, Refrigerating, and Air Conditioning Engineers (ASHRAE) recommends that indoor CO_2 concentrations should be maintained at, or below, 1000 ppm in schools and 800 ppm in offices. Since outdoor CO_2 directly impacts the indoor concentration, an indoor to outdoor differential concentration not greater than about 700 ppm of CO_2, indicates that comfort (odor) criteria related to human bioeffluents are likely to be satisfied. CO_2 concentrations in acceptable outdoor air typically range

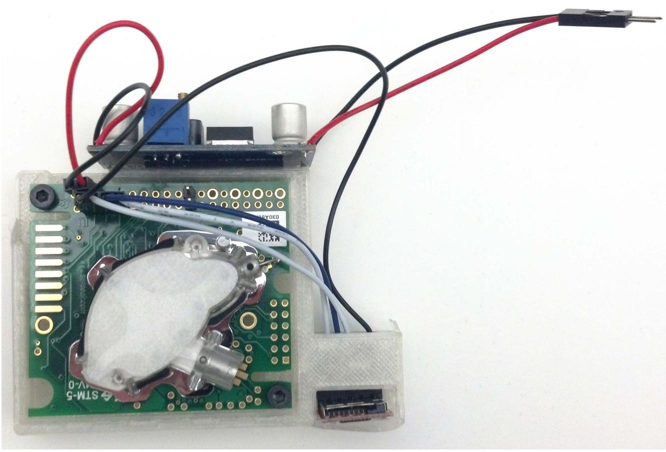

Fig. 2. Data-logging configuration of the K-30 CO_2 sensor used in the experiments. Data are recorded to an SD card for later analysis.

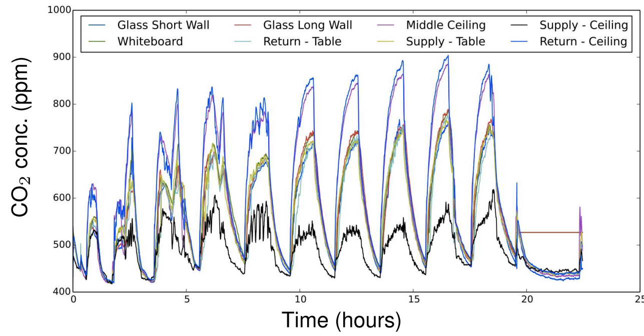

Fig. 3. CO_2 concentrations during Experiment I. Measurements from all eight locations over the approximately 22-h experiment are shown.

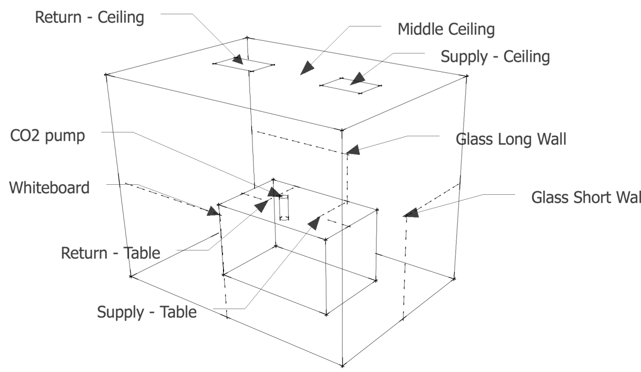

Fig. 4. Locations of the CO_2 sensors and the CO_2 pump inside the conference room during Experiment I.

from 300 to 500 ppm. High CO_2 concentrations in the outdoor air can be an indicator of combustion and/or other contaminant sources [3].

Although it is very difficult to accurately measure CO_2 generation rates by humans, since they can vary widely between different persons depending on current activity, diet, and body size [40], according to the ASHRAE at an activity level of 1.2 met units (1 met $= 18.4$ Btu/h $\times$ ft^2, where Btu is the British thermal unit, an energy unit), corresponding to a sedentary person, the CO_2 generation rate is 0.31 L/min or 0.011 cubic feet/min or 0.66 cubic feet per hour (CFH) [3].

A. Experiment I: Controlled CO_2 Release

In the first experiment, we have the following two goals.

1) To examine the spatial dependence of CO_2 concentration in the room, in particular how well mixed the air is. If there is a spatial dependence, we would like to identify the sensor, which exhibits the most dependence on CO_2 generation in the room.
2) To collect data that can be used for manual or automatic identification of the parameters of a model whose output matches the measured data, when the same CO_2 input is applied to the model and the conference room.

Therefore, our testing methodology is to add a controlled disturbance of CO_2 into the room and measure the resulting response on the sensors placed in the room.

The disturbance input consists of beverage grade (99.9% purity) CO_2 gas being released via a flow regulator at a certain injection rate, and passed through a small 200-W personal heater, to simulate warm breath. A mechanical timer is used to switch the regulator and heater ON and OFF.

We deploy a total of 15 CO_2 sensors in the conference room at eight different locations, as it is shown in Fig. 4. The location of the CO_2 pump during the experiment is also shown in Fig. 4. Note that the CO_2 pump on the z-axis is located approximately 10 cm higher than the table. We choose such a distance to emulate the human behavior because this distance above the table is close to the distance of a human head when a person is sitting on the table inside the conference room. At seven of the eight locations, two CO_2 sensors are colocated for redundancy in case hardware failure makes a reading invalid. We do not encounter any hardware failures during the experiment, so we instead take the mean of redundant measurements.

Fig. 3 shows the sensor readings from a test in which we release CO_2 at a rate of 2 CFH with a 2 h period (1 h ON and 1 h OFF). When CO_2 injection begins, we see clear spatial differences in CO_2 concentrations. During injection, the highest concentrations of 900 ppm are seen by sensors placed at the air return vent and sensors placed on the ceiling at the midpoint between the supply and return vents. The lowest concentrations are seen at the supply vent, which stays below 600 ppm. All of the other sensors, which are placed between chest and waist level in the room, exhibit a similar behavior in response to the CO_2 injection. In general, besides transient behavior due to the changes of ventilation rate, the CO_2 concentrations from different points in the room react the same, albeit with different magnitudes.

To provide a quantified measure of the relation between CO_2 concentrations at different locations in the conference room, we perform an experiment in which we release the CO_2 at a rate of 3 CFH with a period of 30 min (15 min ON/ 15 min OFF). The measured CO_2 concentrations from three different locations in the room are shown in Fig. 5.

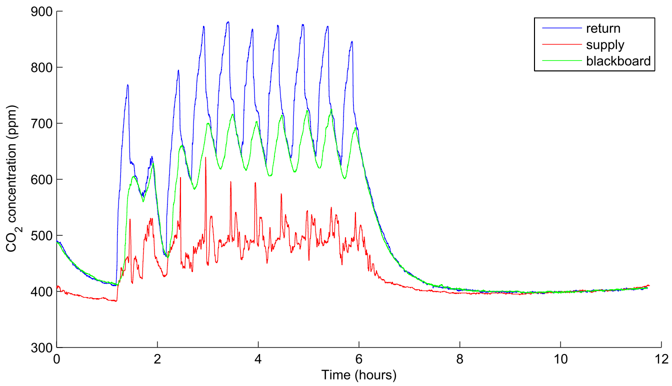

Fig. 5. Measured CO_2 concentration from three different locations inside the conference room for a 0.5-h cycle (0.25 h ON/0.25 h OFF) CO_2 release from a pump.

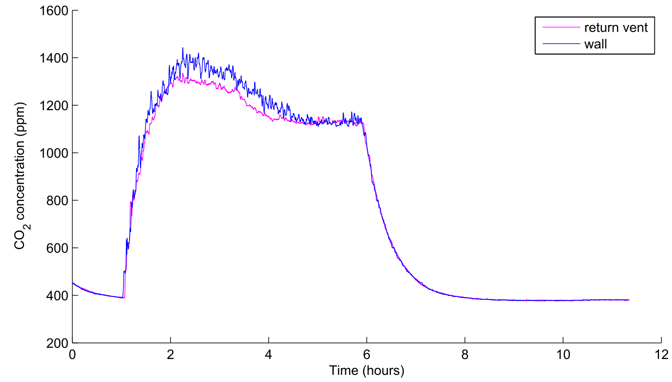

Fig. 6. Measured CO_2 concentration from two different locations inside the conference room for a 5-h CO_2 release from a pump.

TABLE I
CROSS CORRELATION BETWEEN THE MEASUREMENTS SHOWN IN FIG. 5 FROM THREE DIFFERENT LOCATIONS IN THE ROOM

Measurements	Cross-correlation
Return-Supply	0.8966
Return-Blackboard	0.9671
Supply-Blackboard	0.9269

The cross correlation[1] between the measurements from the three different locations is shown in Table I. One can observe that the cross correlation between the return and blackboard measurements is high, whereas the cross correlations that involve supply measurements are lower. This implies that the signals have a high degree of linear dependency (note that when $y_1(k) = c_1 y_2(k) + c_2$, for all k, the cross correlation equals one) on each other, although the correlation with the supply measurements is lower due to the ventilation operation.

One can observe from Fig. 3 that the CO_2 concentrations do not reach a steady state when the CO_2 pump is ON because the ON period is not long enough. We perform an experiment in which we release CO_2 from a pump at a rate of 4 CFH for five consecutive hours and take the measurements from various locations inside the room. In Fig. 6, we show the measured CO_2 concentrations from a sensor at the return vent and from a sensor placed at a blackboard inside the room, for this experiment. One can clearly see the steady-state CO_2 concentration at both the locations, which is about 1150 ppm.

Note that this steady-state concentration might be different than the one for the experiment shown in Fig. 3 since, besides using a different injection rate in each experiment, the steady-state concentration depends on various factors such as the temperature and humidity conditions inside the room, which are different for each experiment, and the ventilation strategy of the conference room, which is different for each experiment and is unknown since the heating, ventilating, and air conditioning operation in the conference room cannot be controlled by the user.

In Fig. 3, one can observe some sudden drops in the CO_2 concentration (for example, at approximately 2.5 h after the onset of the experiment). The drops were caused by either a fault on the mechanical timer that is used to automatically regulate the emission rate of the CO_2 pump (the pins of the mechanical timer did not reach the full position, since the dips are about half an hour after the CO_2 pump is turned ON at each cycle), or by someone opening the door of the conference room (in which the CO_2 pump was located) during the experiment, which caused a sudden drop to the CO_2 concentration due to the difference between the CO_2 concentration inside the conference room and the lower, outside CO_2 concentration. In the experiments with the CO_2 pump shown in Figs. 5 and 6, we do not observe these drops, which reinforces this reasoning.

When the CO_2 injection is turned OFF, all of the sensor measurements at steady state should be identical to the CO_2 concentration of the outside, fresh air, entering the room from the supply vent (i.e., at equilibrium, the air in the room should be well mixed). However, in Fig. 3, we observe the discrepancies in the steady-state concentrations although we performed an offset correction. The reason is that the specific correction method that was used for this experiment, namely, the baseline correction method, is based on offsetting all sensors such that the minimum reading is the same for all sensors, namely, 400 ppm.[2] Yet, if there are some large drops, due to noise, in the measurements that are used for the correction, then the method results in calibration of the actual minimum readings that are higher (since due to the noisy dips, the correction factor overcompensates the offsets) than the minimum baseline of 400 ppm, as well as different for each sensor (despite the fact that both data, i.e., from the experiment and the ones for the correction, are taken with conditions of

[1]The definition of the cross-correlation $r_{y_1 y_2}$ between two signals y_1, y_2 that is employed here is

$$r_{y_1 y_2} = \frac{\sum_{k=1}^{k=T} (y_1(k) - \bar{y}_1)(y_2(k) - \bar{y}_2)}{\sqrt{\sum_{k=1}^{k=T} (y_1(k) - \bar{y}_1)^2} \sqrt{\sum_{k=1}^{k=T} (y_2(k) - \bar{y}_2)^2}} \tag{E1}$$

where $\bar{y}_1$ and $\bar{y}_2$ are the mean values of y_1 and y_2 respectively.

[2]Essentially, sensor readings are taken over a time period and the lowest concentration seen during that period is assumed to be 400 ppm, corresponding to the outdoor air concentration (i.e., the steady-state value if the room is ventilated and no humans are present). The sensor itself performs this correction automatically over a seven and a half day interval. We manually perform this correction by operating all of the sensors overnight, then subtracting an offset from each data set so that the minimum readings from each sensor equaled each other.

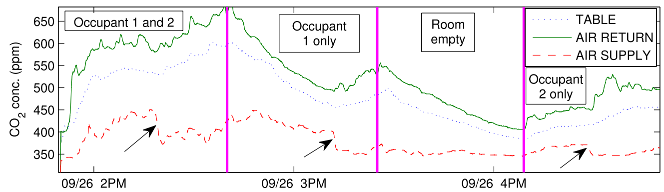

Fig. 7. CO_2 concentrations during Experiment II. Measurements from three locations in the conference room over 3-h experiment are shown. Magenta lines indicate when occupancy changes occurred. The arrows indicate the time instants at which the ventilation rate increases.[3]

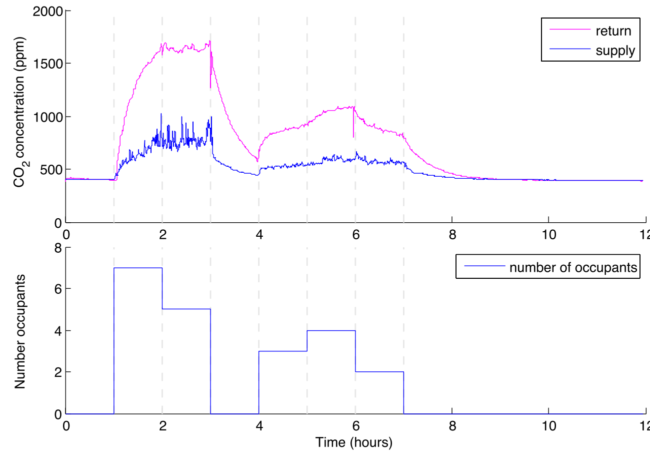

Fig. 8. Top—measured CO_2 concentration at the supply and return vents in the conference room under the presence of humans for Experiment III. Bottom—the number of occupants occupying the conference room during Experiment III.

no CO_2 injection). Upon proper offsetting, which is conducted by setting (for all sensors) the mean of the steady-state value of each sensor to the typical average CO_2 concentration of the outside air, namely, 400 ppm, we can correctly baseline the measurements at steady states at both the start and end of the experiments, as one can observe in Figs. 5 and 6.

From this experiment, we conclude that, when CO_2 is being generated in the room, the concentration of CO_2 local to the air supply represents a mixture of the room's CO_2 concentration and that of the fresh air (about 400 ppm). Other than at the supply vent, we observe that there are large variations on the CO_2 concentration between the points at the ceiling and the points at table height. This is explained by the fact that a warm breath from a human occupant acts as a bubble of gas that rises to the ceiling, since it is more buoyant than the ambient, cooler air. In addition, we observe that there are smaller variations in the CO_2 concentration between different points at the ceiling. Furthermore, we also conclude that, of all the sensors, the measurements most affected by the production of CO_2 are those taken at the air return vent. Therefore, these measurements are the most useful to observe and perform system identification with.

B. Experiment II: Release of CO_2 From a Small Number of Humans

In the second experiment, the goal is to determine the effect of real human occupancy on the concentration of CO_2 in the room. For this experiment, three CO_2 sensors are deployed: 1) at the air supply vent; 2) at the air return vent; and 3) on the conference table at the center of the room. Our excitation procedure consists of adding or removing one of two participants of the experiment, and noting the time that the occupancy changes. Fig. 7 shows a plot of the data gathered from this experiment and when the occupancy transitions occur.

From this plot, we can see the general trend that CO_2 concentration at the conference room table and at the return vent increases when occupants arrive and decreases when occupants leave the room. We also conclude that the concentration at the air supply vent is much less dependent on occupancy. This can be attributed to the constant fresh air ventilation that is provided by building services, so that the fresh air's CO_2 concentration dominates the concentration in the area near the supply vent.

We can also see an interesting effect starting at the approximate times of 2:15 P.M., 3:10 P.M., and 4:20 P.M., at which the CO_2 measurement at the air supply sharply drops corresponding to a rise in CO_2 concentration in the other two measurements. This is attributed to an increase of the ventilation rate. Near to the supply vent, a greater quantity of fresh air mixes with the air near the sensor, driving the concentration down. Moreover, an increase of the air velocity in the room also imparts more turbulent mixing of pockets of CO_2 concentration within the room, pushing them out of the air return, and increasing the concentration at that point. The mixing of these pockets also causes an increase in the CO_2 concentration near the table.

C. Experiment III: Release of CO_2 From a Large Number of Humans

To validate our methodology with a larger number of occupants, we perform a controlled experiment in which we vary the number of occupants in the conference room every 1 h according to the schedule shown in the bottom plot of Fig. 8. The subjects are graduate students with similar physique. The door is closed during the experiment, while the participants are engaged in normal activity such as working on their computers and talking to each other. In the top plot of Fig. 8, we show the measured CO_2 concentrations from the return and supply vents. The behavior of the CO_2 concentration at the return and supply vents is similar to the case of Experiment II.

III. MODEL OF THE CO_2 DYNAMICS

Our model consists of a PDE and an ODE part. The ODE part is given by

$$\dot{X}(t) = -aX(t) + V(t) \tag{1}$$
$$\dot{V}(t) = 0 \tag{2}$$

where X, in ppm, is the source term, which models the effect of the human CO_2 production on the CO_2 concentration

[3]We assume that the air ventilation rate increased at the marked points because an increased proportion of fresh air (typically 400 ppm) would cause a drop in the supply CO_2 concentration. The validity of this hypothesis could be verified by measuring the flow of incoming air at the supply with an anemometer.

(in ppm) of the room [the evolution of which is described later on in (3) and (4) by a convection PDE with a source term], and V is a step-valued function, in ppm/s, representing the CO_2 production rate by the humans inside the room (within the vicinity of humans). Parameter, $1/a$, in units of 100 s, represents a time constant specifying how fast changes to the CO_2 emission rate by the humans affect the CO_2 concentration in the room.

The ODE is coupled with a PDE that models the CO_2 concentration in the room given by

$$u_t(x,t) = -bu_x(x,t) + b_X X(t) \tag{3}$$

$$u(0,t) = 2U_e - U(t) \tag{4}$$

where $u(x,t)$, in ppm, is the concentration of CO_2 in the room at a time $t \geq 0$ and for $0 \leq x \leq 1$, U_e, in ppm, is the steady-state input CO_2 concentration at the supply ventilation, the input U, in ppm, is the measured concentration of the fresh incoming air at the air supply vent, $b > 0$, in $1/100$ s, represents the speed of air convection in the room, and $b_X > 0$, in $1/10^4$ s, specifies the rate of dispersion of CO_2 from the local vicinity of the human to the room. The spatial variable x is unitless and represents a normalized distance along a horizontal axis that connects the air supply and air return. The air supply and air return are located at $x = 0$ and $x = 1$, respectively. Therefore, $u(0,t)$ is the CO_2 concentration inside the room at the location of the air supply and $u(1,t)$ is the CO_2 concentration inside the room at the location of the air return. At the location of the air supply, incoming air is entering the room, and hence, one can view the CO_2 concentration of the fresh incoming air as an input to the system. The air at the location of the air return vent is mixed with CO_2 that convects from the air supply toward the air return, and with CO_2 that is produced from humans. We consider the CO_2 concentration at this point as the output of our system. Any value of the PDE on an interior point of its spatial domain is an indicator of the concentration of CO_2 at the ceiling in a (nonratiometric) normalized distance along an axis from the supply to the return vent.

In Fig. 9, we illustrate the geometrical representation of our model. The PDE part of the model represents convection of air from the air supply to the air return vent near the ceiling. Note the absence of a diffusive term, which we have omitted since it plays a relatively minor role in dispersing indoor pollutants [5]. We choose to model the CO_2 concentrations near the ceiling since this is where we see most effect from human-generated CO_2 (Section II). This is explained by the fact that a warm breath from a human occupant acts as a bubble of gas that rises to the ceiling, since it is more buoyant than the ambient, cooler air. Thus, the air coming from lower in the room is modeled as a source term on the PDE across its entire length. The ODE part of the model (i.e., the filter between the unknown CO_2 emission rate of humans and the CO_2 concentration in the room) intends to model the fact that this bubble of air does not immediately rise to the ceiling but only gradually (which is observed in the response of the CO_2 concentration in the room due to changes of the human's CO_2 input shown in Figs. 7 and 8).

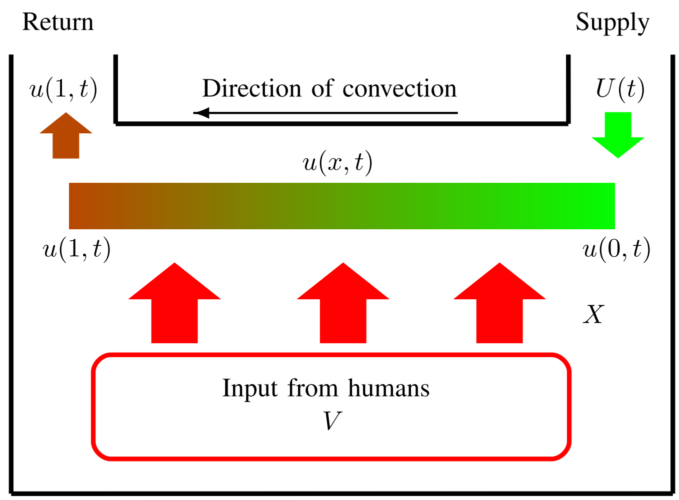

Fig. 9. Geometrical representation of our model (1)–(4). Fresh air (U) enters the room from the supply ventilation. Air near the ceiling (u) convects from the air supply to the air return vent. The humans produce CO_2 (V) that rises (X) to the ceiling.

At $x = 0$, we specify a boundary condition as $u(0,t) = 2U_e - U(t)$ and make the *convention* that the measured, from the sensor located at the air supply vent, CO_2 concentration is U rather than $u(0,t)$ [as in the case of the measured, from the sensor located at the air return vent, CO_2 concentration, which we define as $u(1,t)$] for the following reason. During our experiments, we observed that a sudden drop in the measured CO_2 concentration from the sensor located at the air supply resulted in an increase of the CO_2 concentration at the air return (for example, at the time instants indicated by the arrows in Fig. 7). Hence, for capturing this effect, we define $u(0,t) = U_e - \Delta U(t)$, where $\Delta U(t) = U(t) - U_e$ is the difference of the measured CO_2 concentration at the air supply from its steady-state value. Our explanation for this phenomenon is that a drop in the CO_2 concentration at the supply from its equilibrium value is due to an increase of the airflow of fresh incoming air at the supply vent. The increased airflow has the effect of pushing more pockets of air (carrying CO_2) out of the return vent, resulting into an increase of the CO_2 concentration at the air return.

In Fig. 10, we show the concentration of CO_2 at the air return, as well as the input CO_2 concentration U at the air supply measured by the CO_2 sensors for our first experiment in which we periodically release CO_2 every 1 h. We also show the output $u(1,t)$ of our model with parameters as in Table II and initial condition $u(x,0) = 400$ ppm. For simulating our model, we choose a common one-step backward finite-difference scheme for spatial discretization (with 10 discretization points), whereas we use a simple one-step forward Euler scheme for time discretization (with discretization step $h = 0.01 \times 100$ s). The input V to our model, with which we emulate the behavior of the CO_2 that is released from the pump, is the square wave that is shown in Fig. 11.

In Fig. 12, we show the CO_2 concentration from Experiment II measured by the CO_2 sensors and predicted by the model (1)–(4) with parameters that are shown in Table III, initial condition $u(x,0) = 400$ ppm, and input V that is shown in Fig. 13, with which we emulate the behavior of the CO_2 that

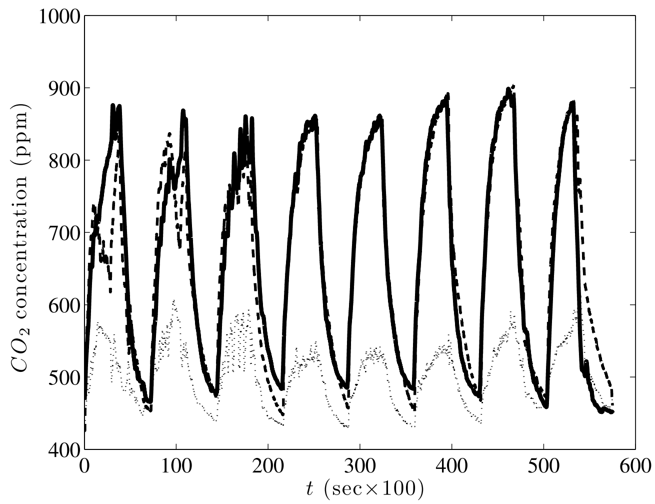

Fig. 10. Solid line—simulated concentration of CO_2 at the air return $u(1,t)$ given by the model (1)–(4) for Fig. 3 of Experiment I. Dashed line—concentration of the CO_2 at the air return measured by the CO_2 sensor, which is shown in Fig. 3. Dotted line—input CO_2 concentration U at the air supply measured by the CO_2 sensor, which is shown in Fig. 3.

TABLE II
PARAMETERS OF THE MODEL (1)–(4) FOR FIG. 3 OF EXPERIMENT I

Physical Paramater	Model parameter	Value
Convection coefficient $\left(\frac{1}{100\text{s}}\right)$	b	0.8
Source term coefficient $\left(\frac{1}{10^4\text{s}}\right)$	b_X	0.2
Time constant of the human's effect (100s)	$\frac{1}{a}$	10
Equilibrium concentration at the air return (ppm)	U_e	450

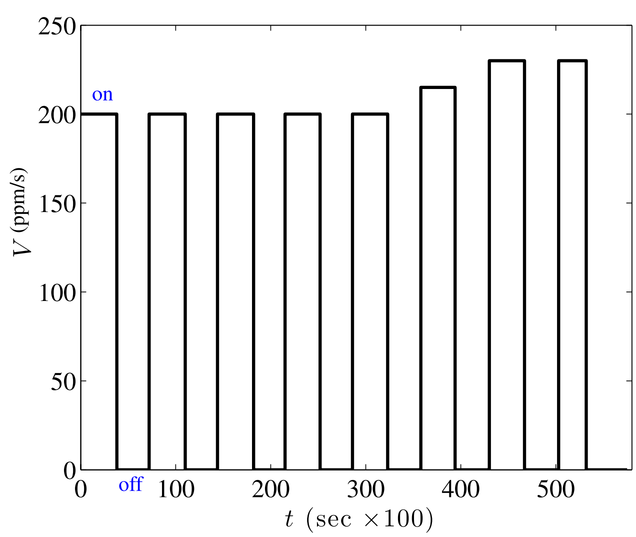

Fig. 11. Input V to the model (1)–(4) from Fig. 3 of Experiment I modeling the concentration of CO_2 that is released from the pump. When $V = 0$, the CO_2 pump is turned OFF and when $V \neq 0$, the CO_2 pump is turned ON.

is produced by humans. Similarly, in Fig. 14, we show the matching of the measured CO_2 concentration at the return to the output $u(1,t)$ of our model (1)–(4) with the parameters shown in Table IV and with the input, which emulates the human emission rate shown in Fig. 15. The matching is reasonably good, fact which validates our model and reinforces its practical importance.

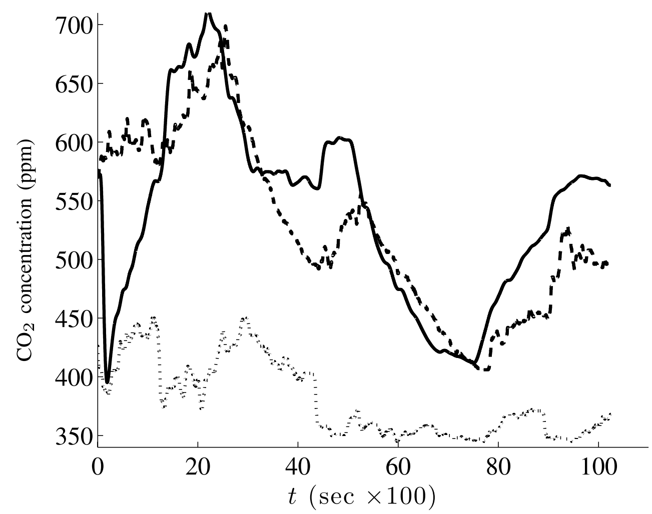

Fig. 12. Solid line—simulated concentration of the CO_2 at the air return $u(1,t)$ given by the model (1)–(4) for Experiment II. Dashed line—concentration of the CO_2 at the air return measured by the CO_2 sensor. Dotted line—input CO_2 concentration U at the air supply measured by the CO_2 sensor.

TABLE III
PARAMETERS OF THE MODEL (1)–(4) FOR EXPERIMENT II

Physical Paramater	Model parameter	Value
Convection coefficient $\left(\frac{1}{100\text{s}}\right)$	b	0.8
Source term coefficient $\left(\frac{1}{10^4\text{s}}\right)$	b_X	0.16
Time constant of the human's effect (100s)	$\frac{1}{a}$	10
Equilibrium concentration at the air return (ppm)	U_e	370

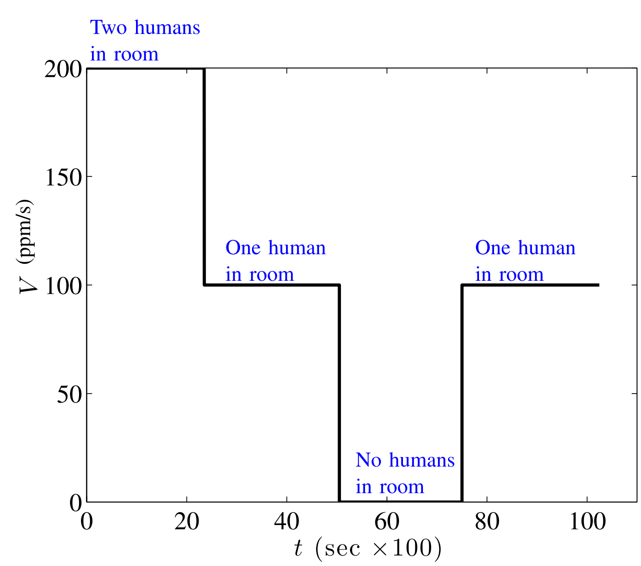

Fig. 13. Input V to the model (1)–(4) *emulating* the *unmeasured* CO_2 generation from the humans for Experiment II.

IV. ESTIMATION OF THE HUMANS' EFFECT

We construct an observer for the plant (1)–(4) assuming the measurements of $u(1,t)$ and $U(t)$, that is, the measurements of the CO_2 concentration at the air return and the air supply vents, respectively. We assume that the parameters

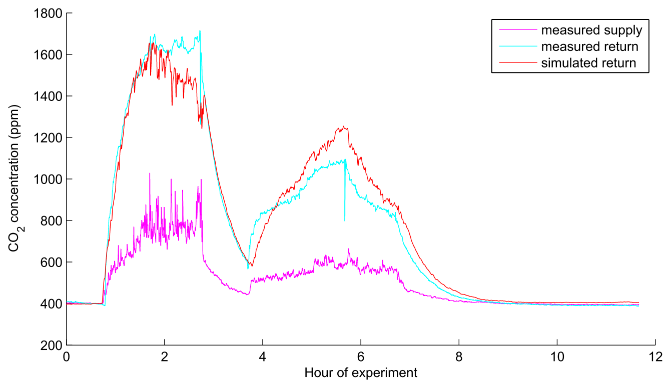

Fig. 14. Matching between the output $u(1, t)$ of the model (1)–(4) with the measured CO_2 concentration at the return under the measured input from the supply ventilation and under the input V shown in Fig. 15.

TABLE IV
PARAMETERS OF THE MODEL (1)–(4) FOR EXPERIMENT III

Physical Paramater	Model parameter	Value
Convection coefficient $\left(\frac{1}{100\text{s}}\right)$	b	1.5
Source term coefficient $\left(\frac{1}{10^4\text{s}}\right)$	b_X	125
Time constant of the human's effect (100s)	$\frac{1}{a}$	20
Equilibrium concentration at the air return (ppm)	U_e	400

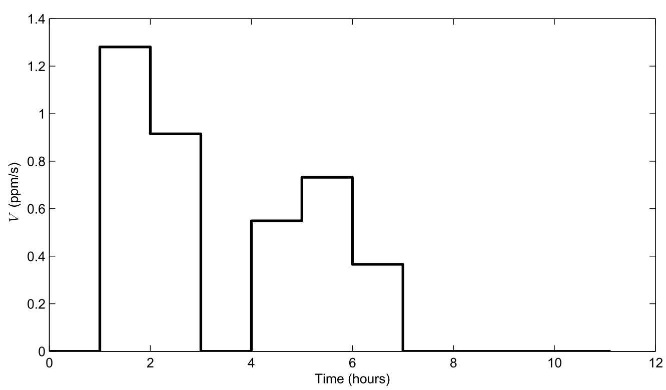

Fig. 15. Input V to the model (1)–(4) *emulating* the *unmeasured* CO_2 generation from the humans for Experiment III.

of the model are known since we manually identify them in Section III.

A. Observer Design

We consider the following observer, which is a copy of the plant (1)–(4) plus output injection:

$$\hat{u}_t(x,t) = -b\hat{u}_x(x,t) + b_X\hat{X}(t) + r(x)(u(1,t) - \hat{u}(1,t)) \tag{5}$$

$$\hat{u}(0,t) = -U(t) + 2U_e \tag{6}$$

$$\dot{\hat{X}}(t) = -a\hat{X}(t) + \hat{V}(t) + L_1(u(1,t) - \hat{u}(1,t)) \tag{7}$$

$$\dot{\hat{V}}(t) = L_2(u(1,t) - \hat{u}(1,t)). \tag{8}$$

The following corollary is a consequence of [7, Th. 2], which deals with linear systems with distributed sensor delays [51].

Corollary 1: Consider the system (1)–(4) and the observer (5)–(8) with

$$r(x) = L_1\pi_1(x) + L_2\pi_2(x) \tag{9}$$

$$\pi_1(x) = \frac{b_X}{a}(e^{\frac{a}{b}x} - 1) \tag{10}$$

$$\pi_2(x) = \frac{b_X}{ba}x + \frac{b_X}{a^2}(1 - e^{\frac{a}{b}x}). \tag{11}$$

Let $b_X \neq 0$ and choose L_1, L_2 such that the matrix $A - \begin{bmatrix} L_1 \\ L_2 \end{bmatrix} C$, where

$$A = \begin{bmatrix} -a & 1 \\ 0 & 0 \end{bmatrix} \tag{12}$$

$$C = [\,\pi_1(1) \quad \pi_2(1)\,] \tag{13}$$

is Hurwitz. Then for any $u_0(x), \hat{u}_0(x) \in L_2(0,1)$, $X(0), \hat{X}(0), V(0), \hat{V}(0) \in \mathbb{R}$, there exist positive constants κ and λ such that the following holds for all $t \geq 0$:

$$\Omega(t) \leq \kappa\Omega(0)e^{-\lambda t} \tag{14}$$

$$\Omega(t) = \int_0^1 (u(x,t) - \hat{u}(x,t))^2 dx + (X(t) - \hat{X}(t))^2 + (V(t) - \hat{V}(t))^2. \tag{15}$$

Proof: In [7], the observer design for the following system is considered:

$$\dot{Z}(t) = AZ(t) \tag{16}$$

$$Y(t) = \int_0^D \bar{C}(\sigma)Z(t-\sigma)d\sigma \tag{17}$$

where $Z \in \mathbb{R}^n$ is the state, $Y \in \mathbb{R}$ is the measured output, and $D \in \mathbb{R}_+$ is a delay. Systems (16), (17) can be written equivalently as

$$\dot{Z}(t) = AZ(t) \tag{18}$$

$$Y(t) = \omega(0,t) \tag{19}$$

where

$$\omega_t(z,t) = \omega_z(z,t) + \bar{C}(z)Z(t) \tag{20}$$

$$\omega(D,t) = 0. \tag{21}$$

One can see this by noting that the solution to (20) and (21) is $\omega(z,t) = \int_z^D \bar{C}(\sigma)Z(t+z-\sigma)d\sigma$. We show next that system (1)–(4) can be written in the form of system (18)–(21), and hence, one can then apply in [7, Th. 2]. Performing the following change of variables to the spatial variable x:

$$z = \frac{1-x}{b}, \tag{22}$$

and defining $D = 1/b$, $Z = [\,X \;\; V\,]^T$, $u(1-bz,t) = \omega(z,t)$, and $\bar{C} = [\,b_X \;\; 0\,]$, we write system (1)–(4) as

$$\dot{Z}(t) = AZ(t) \tag{23}$$

$$\omega_t(z,t) = \omega_z(z,t) + \bar{C}(z)Z(t) \tag{24}$$

$$\omega(D,t) = -U(t) + 2U_e. \tag{25}$$

Systems (23)–(25) is of the form (18), (20), and (21) with the difference of the nonhomogenous boundary condition at $z = D$. However, the result in [7] applies with the trivial

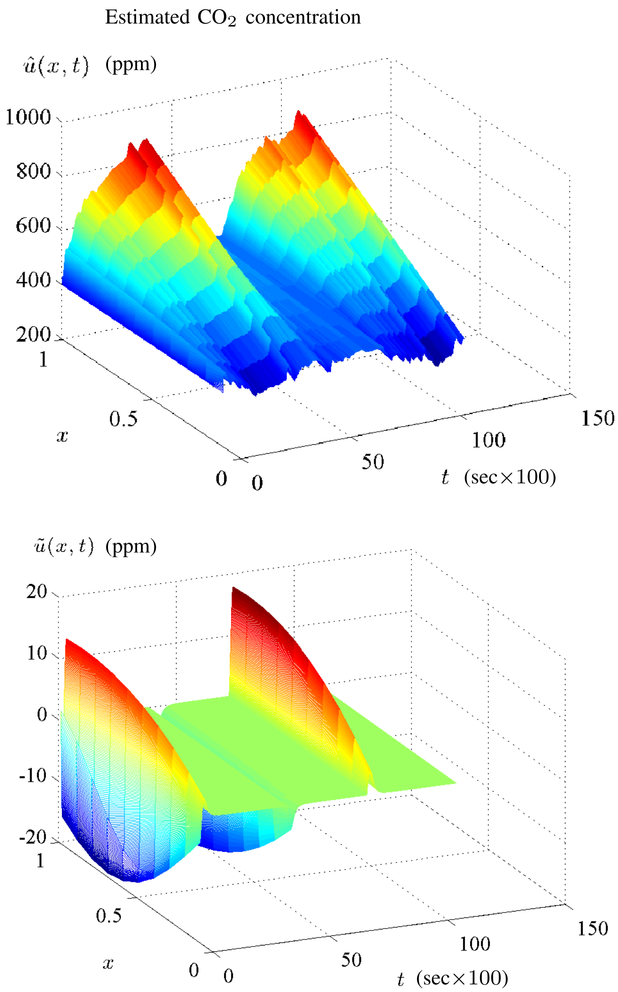

Fig. 16. Top—estimation $\hat{u}(x,t)$ of the CO_2 concentration in the room $u(x,t)$, as it is produced by the model (1)–(4), for Fig. 3 of Experiment I. Bottom—error $\tilde{u}(x,t) = u(x,t) - \hat{u}(x,t)$ of the estimation of the CO_2 concentration in the room, as it is produced by the model (1)–(4), for Fig. 3 of Experiment I (shown after 1×100 s for a better visualization).

modification $\hat{\omega}(D,t) = -U(t) + 2U_e$ instead of $\hat{\omega}(D,t) = 0$ in relation (6) of the observer design (5)–(8), to account for the additional measured input. Defining $L = \begin{bmatrix} L_1 & L_2 \end{bmatrix}^T$, the observer (5)–(8) can be written in the (Z,ω) variables as

$$\dot{\hat{Z}}(t) = A\hat{Z}(t) + L(\omega(0,t) - \hat{\omega}(0,t)) \tag{26}$$

$$\hat{\omega}_t(z,t) = \hat{\omega}_z(z,t) + \bar{C}(z)\hat{Z}(t) + r(1-bz)(\omega(0,t) - \hat{\omega}(0,t)) \tag{27}$$

$$\hat{\omega}(D,t) = -U(t) + 2U_e. \tag{28}$$

The stability proof of [7, Th. 2] is based on the dynamics of the error system, namely, on the dynamics of $\omega - \hat{\omega}$ and $Z - \hat{Z}$. We show next that the error system is identical to the error system in [7]. Combining (18), (20), and (21) with (26)–(28) and since $r(x) = [\pi_1(x) \quad \pi_2(x)]L$, we obtain that

$$\dot{\tilde{Z}}(t) = A\tilde{Z}(t) - L\tilde{\omega}(0,t) \tag{29}$$

$$\tilde{\omega}_t(z,t) = \tilde{\omega}_z(z,t) + \bar{C}(z)\tilde{Z}(t) - [\,\pi_1(1-bz)\ \pi_2(1-bz)\,]L\tilde{\omega}(0,t) \tag{30}$$

$$\tilde{\omega}(D,t) = 0 \tag{31}$$

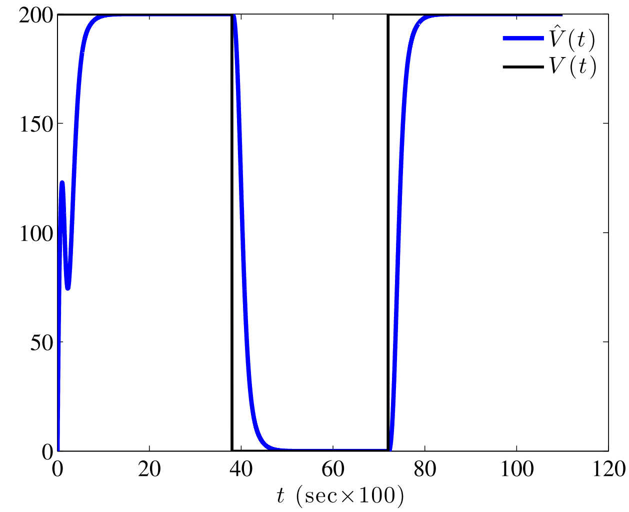

Fig. 17. Estimation $\hat{V}$ (blue line) of the pump input V (black line) in Fig. 11 for Fig. 3 of Experiment I.

which is the same error system, as in [7]. We show next that the observability condition of [7, Th. 2] of the pair $(A, \int_0^D \bar{C}(\sigma)e^{-A\sigma}d\sigma)$ is equivalent to the observability condition of Corollary 1, i.e., the observability of the pair (A, C). This follows by noting that:

$$\begin{aligned}\int_0^D \bar{C}(\sigma)e^{-A\sigma}d\sigma &= \frac{b_X}{a}\int_0^{\frac{1}{b}} [a e^{a\sigma} \quad 1 - e^{a\sigma}]d\sigma \\ &= \frac{b_X}{a}\left[e^{\frac{a}{b}} - 1 \quad \frac{1}{b} + \frac{1}{a}(1 - e^{\frac{a}{b}})\right] = C.\end{aligned} \tag{32}$$

Therefore, to apply [7, Th. 2], it remains to show that when $b_X \neq 0$, the pair (A, C) is observable (in which case one can choose L_1 and L_2 such that the matrix $A - \begin{bmatrix} L_1 \\ L_2 \end{bmatrix} C$ is Hurwitz). The determinant of the observability matrix O of the pair (A, C) is $\det(O) = \pi_1(1)(\pi_1(1) + a\pi_2(1))$. Using (10) and (11), it follows that $\det(O) \neq 0$ whenever $b_X \neq 0$. ■

B. Simulations

We test our observer design for the model (1)–(4). We apply the input U that is measured from the sensor and the input V, which is shown in Figs. 11 and 13, and *emulates* the CO_2 generation from the pump and the (*unmeasured*) CO_2 generation from the humans, respectively, for each of the two experiments. We choose the initial conditions for the observer as $\hat{u}(x,0) = 400$, for all $x \in [0,1]$, and $\hat{X}(0) = \hat{V}(0) = 0$. We choose the observer gains as $L_1 = 9.5$, $L_2 = 4$, such that the matrix $A - \begin{bmatrix} L_1 \\ L_2 \end{bmatrix} C$, where A and C are defined in (12) and (13), respectively, has two eigenvalues at -1. In Fig. 16, we show the estimation of the state u together with the estimation error $\tilde{u} = u - \hat{u}$, which converges to zero, and in Fig. 17, we show the estimation of the input V from the pump for the first 110×100 s for Fig. 3 of Experiment I, which converges to the true value of V. Using the same initial

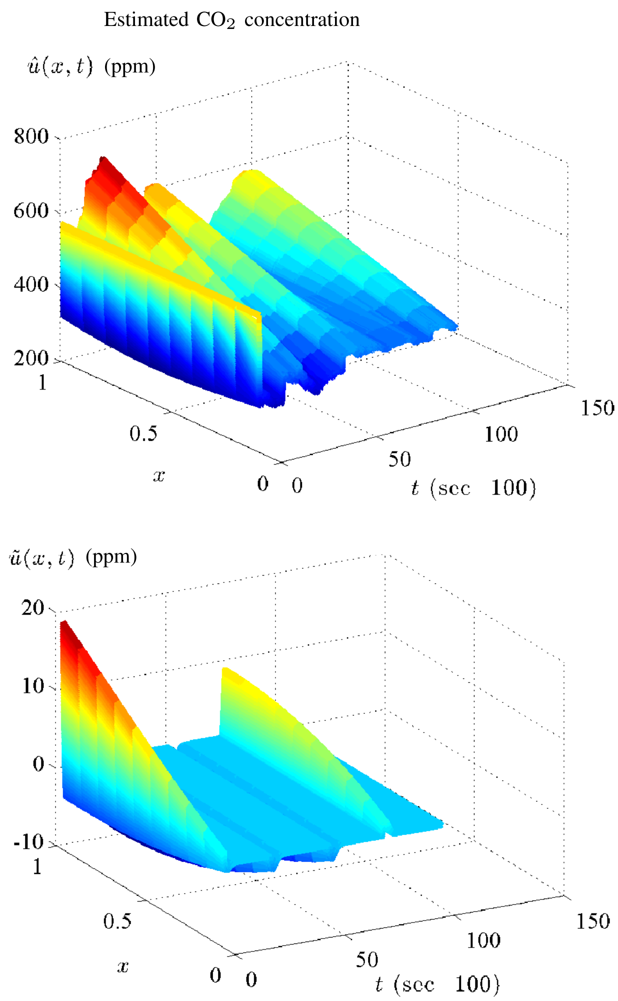

Fig. 18. Top—estimation $\hat{u}(x,t)$ of the CO_2 concentration in the room $u(x,t)$, as it is produced by the model (1)–(4), for Experiment II. Bottom—error $\tilde{u}(x,t) = u(x,t) - \hat{u}(x,t)$ of the estimation of the CO_2 concentration in the room, as it is produced by the model (1)–(4), for Experiment II (shown after 3×100 s for a better visualization).

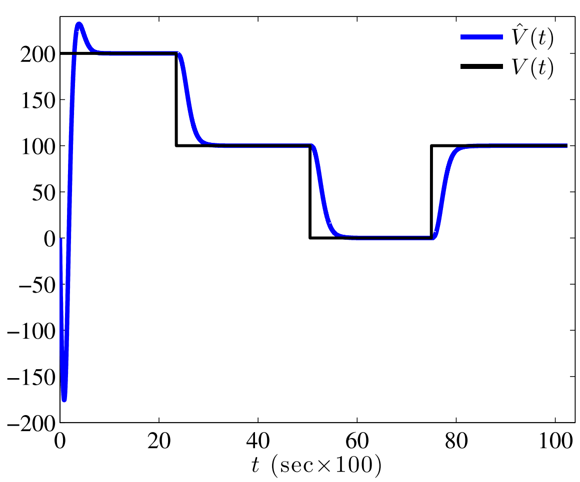

Fig. 19. Estimation $\hat{V}$ (blue line) of the input V (black line) in Fig. 13 *emulating* the *unmeasured* CO_2 concentration that is produced from the people for Experiment II.

conditions for the observer and the same observer's gains as in Fig. 3 of Experiment I (but since b_X is different for Experiment II the matrix $A - \begin{bmatrix} L_1 \\ L_2 \end{bmatrix} C$ has now eigenvalues located at $-0.8012 \pm 0.3976i$), we show in Fig. 18, the estimation of the state u together with the estimation error $\tilde{u}$, and in Fig. 19 the estimation of the input V produced by the people for Experiment II.

V. Conclusion

In this paper, we developed a PDE-ODE model that describes the dynamics of the CO_2 concentration in a conference room. We validated our model by conducting two different experiments. We designed and validated an observer for the estimation of the unknown CO_2 input that is generated by humans.

Future work will address the problem of estimation of the actual human occupancy level using the measurements of CO_2. This is a highly nontrivial problem because humans' CO_2 generation rates can vary widely between different persons depending on current activity, diet, and body size [39].

It is also crucial to develop online identifiers for the parameters of the model, since these parameters change with time due to their dependency on time-varying quantities such as heat generation [5]. For example, it is shown in [5] that the mixing time of a pollutant, generated from a point source, in a room can vary depending on the sunlight energy input in the room. A starting point for such a study could be the swapping identifiers that are developed in [42] and [44] for parabolic PDEs and applied in [33] for the identification of the state-of-health of batteries, and the update laws designed in [8]–[12], for the estimation of unknown plant parameters and delays in adaptive control of linear delay systems.

Another topic for future research is to combine the observer design developed in this paper with parameter identifiers that are designed using only output measurements. In other words, to design an adaptive observer [20], [23] using the observer design presented in this paper as a first step. However, for PDE systems, this is far from trivial due to the lack of systematic procedures for the construction of state transformations that can transform the original system to a system having an observer canonical form [20], [42], [45], [46] in which, the unknown parameters multiply the measured outputs. For this reason, designing adaptive observers for PDE systems is possible only in special cases [42]. As an alternative, one could resort to finite-dimensional approximations as it is done, for example, in [35].

Acknowledgment

The authors would like to thank W. W. Nazaroff and D. Rim for their useful discussions and for pointing out some important literature on the topics of indoor airflow modeling and of indoor contaminant source identification.

References

[1] Y. Agarwal, B. Balaji, S. Dutta, R. K. Gupta, and T. Weng, "Duty-cycling buildings aggressively: The next frontier in HVAC control," in *Proc. IEEE Conf. Inf. Process. Sensor Netw.*, Apr. 2011, pp. 246–257.

[2] S. Amin, X. Litrico, S. S. Sastry, and A. M. Bayen, "Cyber security of water SCADA systems—Part II: Attack detection using enhanced hydrodynamic models," *IEEE Trans. Control Syst. Technol.*, vol. 21, no. 5, pp. 1679–1693, Sep. 2012.

[3] *Ventilation for Acceptable Indoor Air Quality*, ASHRAE Standard 62, 1999.

[4] A. Bastani, F. Haghighat, and J. A. Kozinski, "Contaminant source identification within a building: Toward design of immune buildings," *Building Environ.*, vol. 51, pp. 320–329, May 2012.

[5] A. V. Baughman, A. J. Gadgil, and W. W. Nazaroff, "Mixing of a point source pollutant by natural convection flow within a room," *Indoor Air*, vol. 4, no. 2, pp. 114–122, 1994.

[6] N. Bedjaoui, X. Litrico, D. Koenig, and P. O. Malaterre, "H_∞ observer for time-delay systems: Application to FDI for irrigation canal," in *Proc. IEEE Conf. Decision Control*, San Diego, CA, USA, Dec. 2006, pp. 532–537.

[7] N. Bekiaris-Liberis and M. Krstic, "Lyapunov stability of linear predictor feedback for distributed input delays," *IEEE Trans. Autom. Control*, vol. 56, no. 3, pp. 655–660, Mar. 2011.

[8] N. Bekiaris-Liberis and M. Krstic, "Delay-adaptive feedback for linear feedforward systems," *Syst. Control Lett.*, vol. 59, no. 5, pp. 277–283, 2010.

[9] N. Bekiaris-Liberis, M. Jankovic, and M. Krstic, "Adaptive stabilization of LTI systems with distributed input delay," *Int. J. Adapt. Control Signal Process.*, vol. 27, nos. 1–2, pp. 46–65, 2013.

[10] D. Bresch-Pietri, J. Chauvin, and N. Petit, "Adaptive control scheme for uncertain time-delay systems," *Automatica*, vol. 48, no. 8, pp. 1536–1552, 2012.

[11] D. Bresch-Pietri and M. Krstic, "Delay-adaptive predictor feedback for systems with unknown long actuator delay," *IEEE Trans. Autom. Control*, vol. 55, no. 9, pp. 2106–2112, Sep. 2010.

[12] D. Bresch-Pietri and M. Krstic, "Adaptive trajectory tracking despite unknown input delay and plant parameters," *Automatica*, vol. 45, no. 9, pp. 2074–2081, 2009.

[13] H. Cai, X. Li, Z. Chen, and L. Kong, "Fast identification of multiple indoor constant contaminant sources by ideal sensors: A theoretical model and numerical validation," *Indoor Built Environ.*, vol. 22, pp. 897–909, Sep. 2013.

[14] C. Y. H. Chao and J. S. Hu, "Development of a dual-mode demand control ventilation strategy for indoor air quality control and energy saving," *Building Environ.*, vol. 39, no. 4, pp. 385–397, 2004.

[15] Q. Chen, "Ventilation performance prediction for buildings: A method overview and recent applications," *Building Environ.*, vol. 44, no. 4, pp. 848–858, 2009.

[16] F. Di Meglio, R. Vazquez, and M. Krstic, "Stabilization of a system of $n+1$ coupled first-order hyperbolic linear PDEs with a single boundary input," *IEEE Trans. Autom. Control*, vol. 58, no. 12, pp. 3097–3111, Dec. 2013.

[17] F. Di Meglio, D. Bresch-Pietri, and U. J. F. Aarsnes, "An adaptive observer for hyperbolic systems with application to underbalanced drilling," in *Proc. IFAC World Congr.*, Cape Town, South Africa, 2014, pp. 11391–11397.

[18] Department of Energy (DoE). (2010). *Energy Efficiency Trends in Residential and Commercial Buildings*. [Online]. Available: http://apps1.eere.energy.gov/buildings/publications/pdfs/corporate/building_trends_2010.pdf

[19] V. L. Erickson, M. A. Carreira-Perpinan, and A. E. Cerpa, "OBSERVE: Occupancy-based system for efficient reduction of HVAC energy," in *Proc. IEEE Conf. Inf. Process. Sensor Netw.*, Apr. 2011, pp. 258–269.

[20] P. A. Ioannou and J. Sun, *Robust Adaptive Control*. Englewood Cliffs, NJ, USA: Prentice-Hall, 1996.

[21] C. C. Federspiel, "Estimating the inputs of gas transport processes in buildings," *IEEE Trans. Control Syst. Technol.*, vol. 5, no. 5, pp. 480–489, Sep. 1997.

[22] D. Koenig, N. Bedjaoui, and X. Litrico, "Unknown input observers design for time-delay systems application to an open-channel," in *Proc. 44th IEEE Conf. Decision Control*, Seville, Spain, Dec. 2005, pp. 5794–5799.

[23] M. Krstic, I. Kanellakopoulos, and P. V. Kokotovic, *Nonlinear and Adaptive Control Design*. New York, NY, USA: Wiley, 1995.

[24] M. Krstic and A. Smyshlyaev, *Boundary Control of PDEs: A Course on Backstepping*. Philadelphia, PA, USA: SIAM, 2008.

[25] M. Krstic and A. Smyshlyaev, "Backstepping boundary control for first-order hyperbolic PDEs and application to systems with actuator and sensor delays," *Syst. Control Lett.*, vol. 57, no. 9, pp. 750–758, 2008.

[26] (2013). *K-30 10,000 ppm CO_2 Sensor*. [Online]. Available: http://co2meters.com/Documentation/Datasheets/DS30-01%20-%20K30.pdf

[27] K. P. Lam *et al.*, "Occupancy detection through an extensive environmental sensor network in an open-plan office building," in *Proc. 11th Int. IBPSA Building Simulation*, 2009, pp. 1452–1459.

[28] Y. Li and P. V. Nilsen, "CFD and ventilation research," *Indoor Air*, vol. 21, no. 6, pp. 442–453, 2011.

[29] W.-J. Liu and M. Krstic, "Adaptive control of Burgers' equation with unknown viscosity," *Int. J. Adapt. Control Signal Process.*, vol. 15, no. 7, pp. 745–766, 2001.

[30] X. Liu and Z.-J. Zhai, "Protecting a whole building from critical indoor contamination with optimal sensor network design and source identification methods," *Building Environ.*, vol. 44, no. 11, pp. 2276–2283, 2009.

[31] A. C. Megri and F. Haghighat, "Zonal modeling for simulating indoor environment of buildings: Review, recent developments, and applications," *HVAC&R Res.*, vol. 13, no. 6, pp. 887–905, 2007.

[32] L. Mora, A. J. Gadgil, and E. Wurtz, "Comparing zonal and CFD model predictions of isothermal indoor airflows to experimental data," *Indoor Air*, vol. 13, no. 2, pp. 77–85, 2003.

[33] S. J. Moura, N. A. Chaturvedi, and M. Krstic, "PDE estimation techniques for advanced battery management systems—Part II: SOH identification," in *Proc. Amer. Control Conf.*, Jun. 2012, pp. 566–571.

[34] S. J. Moura, N. A. Chaturvedi, and M. Krstic, "PDE estimation techniques for advanced battery management systems—Part I: SOC estimation," in *Proc. Amer. Control Conf.*, Jun. 2012, pp. 559–565.

[35] S. J. Moura, M. Krstic, and N. A. Chaturvedi, "Adaptive PDE observer for battery SOC/SOH estimation via an electrochemical model," *ASME J. Dyn. Syst., Meas., Control*, vol. 136, no. 1, p. 011015, 2014.

[36] W. W. Nazaroff and G. R. Cass, "Mathematical modeling of indoor aerosol dynamics," *Environ. Sci. Technol.*, vol. 23, no. 2, pp. 157–166, 1989.

[37] National Environment Agency (NEA). (2007). *E^2 Singapore*. [Online]. Available: http://www.nea.gov.sg/cms/ccird/E2%20Singapore%20%28for%20upload%29.pdf

[38] S.-T. Parker and V. Bowman, "State-space methods for calculating concentration dynamics in multizone buildings," *Building Environ.*, vol. 46, no. 8, pp. 1567–1577, 2011.

[39] A. K. Persily, "Evaluating building IAQ and ventilation with indoor carbon dioxide," *Trans. Amer. Soc. Heating Refrig. Air Conditioning Eng.*, vol. 103, no. 2, pp. 193–204, 1997.

[40] O. A. Seppanen, W. J. Fisk, and M. J. Mendell, "Association of ventilation rates and CO_2 concentrations with health and other responses in commercial and institutional buildings," *Indoor Air*, vol. 9, no. 4, pp. 226–252, 1999.

[41] M. D. Sohn, P. Reynolds, N. Singh, and A. J. Gadgil, "Rapidly locating and characterizing pollutant releases in buildings," *J. Air Waste Manage. Assoc.*, vol. 52, no. 12, pp. 1422–1432, 2002.

[42] A. Smyshlyaev and M. Krstic, *Adaptive Control of Parabolic PDEs*. Princeton, NJ, USA: Princeton Univ. Press, 2010.

[43] A. Smyshlyaev and M. Krstic, "Backstepping observers for a class of parabolic PDEs," *Syst. Control Lett.*, vol. 54, no. 7, pp. 613–625, 2005.

[44] A. Smyshlyaev and M. Krstic, "Adaptive boundary control for unstable parabolic PDEs—Part II: Estimation-based designs," *Automatica*, vol. 43, no. 9, pp. 1543–1556, 2007.

[45] A. Smyshlyaev and M. Krstic, "Adaptive boundary control for unstable parabolic PDEs—Part III: Output feedback examples with swapping identifiers," *Automatica*, vol. 43, no. 9, pp. 1557–1564, 2007.

[46] A. Smyshlyaev, Y. Orlov, and M. Krstic, "Adaptive identification of two unstable PDEs with boundary sensing and actuation," *Int. J. Adapt. Control Signal Process.*, vol. 23, no. 2, pp. 131–149, 2009.

[47] V. Vukovic and J. Srebric, "Application of neural networks trained with multizone models for fast detection of contaminant source position in buildings," *ASHRAE Trans.*, vol. 113, pp. 154–162, Jul. 2007.

[48] V. Vukovic, P. C. Tabares-Velasco, and J. Srebric, "Real-time identification of indoor pollutant source positions based on neural network locator of contaminant sources and optimized sensor networks," *Air Waste Manage. Assoc.*, vol. 60, no. 9, pp. 1034–1048, 2010.

[49] S. Wang and X. Jin, "CO_2-based occupancy detection for on-line outdoor air flow control," *Indoor Built Environ.*, vol. 7, no. 3, pp. 165–181, 1998.

[50] T. F. Zhang and Q. Chen, "Identification of contaminant sources in enclosed environments by inverse CFD modeling," *Indoor Air*, vol. 17, no. 3, pp. 167–177, 2007.

[51] Q.-C. Zhong, *Robust Control of Time-Delay Systems*. New York, NY, USA: Springer-Verlag, 2006.

Kevin Weekly received the B.S. degree in electrical engineering and computer sciences from the University of Texas at Dallas, Dallas, TX, USA, and the Ph.D. degree in electrical engineering and computer sciences from the University of California at Berkeley, Berkeley, CA, USA.

He is currently a Research Scientist with Fitbit, Inc., San Francisco, CA, USA. His current research interests include distributed autonomous robotics, wireless sensor networks, and estimation and control for embedded systems, with particular applications to indoor environmental sensing to reduce energy use of office buildings and environmental sensing of water networks.

Nikolaos Bekiaris-Liberis received the Ph.D. degree from the University of California at San Diego, La Jolla, CA, USA, in 2013.

He is currently a Post-Doctoral Researcher with the University of California at Berkeley, Berkeley, CA, USA. He has co-authored the SIAM book entitled *Nonlinear Control Under Nonconstant Delays*. His current research interests include delay systems, distributed parameter systems, nonlinear control, and their applications.

Dr. Bekiaris-Liberis was a finalist for the Student Best Paper Award at the 2010 ASME Dynamic Systems and Control Conference and the 2013 IEEE Conference on Decision and Control. He was a recipient of the Chancellor's Dissertation Medal in Engineering from the University of California at San Diego in 2014.

Ming Jin received the B.Eng. (Hons.) degree in electronic and computer engineering from the Hong Kong University of Science and Technology, Hong Kong, in 2012. He is currently pursuing the Ph.D. degree in electrical engineering and computer science with the University of California at Berkeley, Berkeley, CA, USA.

His current research interests include energy efficient buildings, statistical learning, and control theory, with particular applications to indoor positioning, occupancy estimation, activity recognition, and social game for energy savings.

Alexandre M. Bayen received the Engineering degree from École Polytechnique, Palaiseau, France, and the M.S. and Ph.D. degrees from Stanford University, Stanford, CA, USA.

He was a Visiting Researcher with the NASA Ames Research Center, Mountain View, CA, USA, from 2000 to 2003, and the Director of the Autonomous Navigation Laboratory with the Laboratoire de Recherches Balistiques et Aerodynamiques, Ministere de la Defense, Vernon, France, where he holds the rank of Major. He is currently a Chancellor Professor of Electrical Engineering and Computer Science and Civil and Environmental Engineering with the University of California at Berkeley, Berkeley, CA, USA. He is the Director of the Institute for Transportation Studies. He has authored two books and over 150 articles in peer-reviewed journals and conferences.

Dr. Bayen received the CAREER Award from the National Science Foundation, the Best of ITS Award for Best Innovative Practice, (2008 ITS World Congress), the TRANNY Award (California Transportation Foundation), the PECASE Award (The White House), the Huber Prize (ASCE), the Ruberti Prize (IEEE), and the Okawa Research Grant Award.